

**THE MESHLESS APPROACH FOR THE CELL METHOD:
A NEW WAY FOR THE NUMERICAL SOLUTION OF
DISCRETE CONSERVATION LAWS**

LUIGINO ZOVATTO

*Dipartimento di Ingegneria Civile, University of Trieste, via Valerio 6/1
Trieste, 34127, Italy*

E-mail: zovatto@dic.univ.trieste.it

and

MATTEO NICOLINI

*Dipartimento di Georisorse e Territorio, University of Udine, via Cotonificio 114
Udine, 33100, Italy*

E-mail: nicolini@dgt.uniud.it

Received (received date)

Revised (revised date)

A new methodology for the solution of discrete conservation laws, based on a point by point approach, is presented. For each node, a local mesh is firstly generated, made up of all triangles whose vertices coincide with the node itself and its neighbours. The solution is then determined through mass, energy and momentum balances directly written in a discrete form over a tributary region, represented by the polygon whose vertices are the barycenters and/or the circumcenters of the triangles belonging to the local mesh. This approach avoids global mesh generation (computationally much more expensive), and is particularly efficient for non-linear problems, such as fracture mechanics. In the paper, the numerical method is described in detail for Laplace equation, together with the convergence order as a function of the number of nodes and the type of boundary conditions. Finally, in order to further simplify the procedure, it is proposed to consider the tributary area formed by the circle with center in the generic node and radius equal to the average of the distances between the node and its neighbours. This results in a considerable ease in writing the discrete form of the governing equations, while maintaining the same accuracy and order of convergence.

Keywords: Discrete formulation; Cell Method; Meshless Approach; FEM.

1. Introduction

In these last years, discrete formulation of field theories, that is, a formulation starting directly from *global* quantities and not relying, as usually, on the discretization of the corresponding differential form, is gaining an ever-increasing popularity, due to its promising results. Global quantities are related to spatial and temporal enti-

ties having an extension: electric voltage is related to a line, heat flux to a surface, energy to a volume, impulse to a time interval. Global quantities are thus functions of a line, a surface, a volume, a time interval: in other words, they are *set* (or *domain*) functions. Global quantities are often called *integral* quantities, but they are not meant to be considered as integrals of field functions. For instance, the mass in a volume of space has not to be necessarily thought as the integral of the density.

Classical differential formulation relies on field functions, and is dependent on coordinate systems. The discrete approach is radically different, in that governing physical laws are directly written in discrete form, through the use of global quantities. In particular, the recently introduced Cell Method (CM) has a widespread range of applicability, with results in some cases better than those obtained by Finite Differences (FD) or Finite Element Method (FEM).^{1,2,3} To this end, two systems of cells have to be adopted, being dual one another. The computational domain is firstly subdivided into many elementary cells (the so-called *primal* mesh) and, for these, a second (the *dual*) mesh is constructed, as described later. The dual mesh provides the geometrical entities in which discrete conservation and circuital laws are written.

In the last decade, and particularly in these last years, FEM world has seen the growth of many meshless approaches.^{4,5,6,7,8,9,10} Some of them were aimed at encompassing typical problems encountered when analyzing, for example, fracture propagation in elasticity: mesh generation at every step is actually a time consuming and computationally intensive process. First works of this kind are at the beginning of the 90's, and Belytscko et al. (1996) have provided a thorough state-of-the-art of these methodologies.¹¹ However, meshless methods are not free from problems, especially when imposing Dirichlet boundary conditions, and various researchers have proposed different solutions, less or more satisfactory.^{12,13}

There is a number of works on fracture propagation analysis based on the discrete formulation.^{14,15} Since there are many analogies between the Cell Method and the Finite Element Method, the aim of this paper was to investigate the applicability and the performance of the meshless approach within the discrete formulation.

2. An example of discrete formulation: the Poisson equation

The Cell Method derives the discrete formulation of governing laws by applying conservation equations (mass, momentum, energy) to a well-defined geometrical entity of the computational domain. CM provides a framework for a correct relationship between physical quantities and geometrical entities of the primal and dual mesh. As an example, let us analyze the two-dimensional case, and assume triangular cells forming the primal mesh, as shown in Fig. 1a. If, for every cell, we consider one particular point (like the barycenter, the circumcenter, or the incenter), another system of cells can be straightforwardly generated, made up of polygons whose sides are the connections of contiguous points of the triangles. Thus, together with the Delaunay triangulation (primal mesh), there is a dual mesh unambiguously identified. Fig. 1b

represents the Voronoi dual mesh, obtained when the circumcentre of each triangle is considered: in this case, the two meshes are complementary structures with the characteristic that the sides of the primal are perpendicular to those of the dual. Another dual mesh can be formed by the polygons whose sides are the connections between the barycenter of each triangle and the midpoint of their sides (Fig. 1c): also in this case the two meshes are complementary and biunivocally identified. The above considerations show that the Cell Method gives the possibility of choosing the tributary (or influence) regions of every node, also called tributary areas or *dual polygons*. The Finite Element Method lacks of this operational freedom.

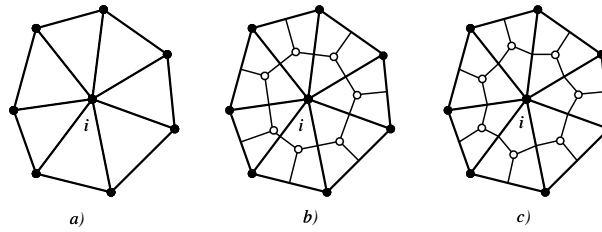


Fig. 1. Example of primal and dual meshes, and of tributary region of node i : a) triangular primal mesh; b) primal (thin line) and dual (thick line) meshes, with dual mesh obtained connecting the circumcenters of the triangles; c) same as b), but with dual mesh formed using the barycenters.

Let us examine the typical problem of heat conduction, in which temperatures are associated with the nodes of the primal mesh. Discrete formulation is obtained from Fourier's law according to which the heat flux crossing a surface in the unit time is proportional to the area of the surface and the temperature gradient component along the normal:

$$\phi = -k \nabla T \cdot \vec{n} A \quad (1)$$

or, equivalently,

$$\phi = -k \frac{\Delta T}{L} A \quad (2)$$

if $\vec{L} \perp \vec{A}$, where \vec{n} is the normal to surface of area A , and L is the distance between the points whose temperature difference is ΔT . Referring now to Fig. 2, the Poisson equation can be written as

$$- \sum_{e \in \mathcal{J}(i)} k \left(\vec{g}^e \cdot \vec{A}_{ik}^e + \vec{g}^e \cdot \vec{A}_{ij}^e \right) = \phi_i^c + \phi_i^p \quad (3)$$

where \vec{A}_{ik}^e and \vec{A}_{ij}^e represent the area vectors of the i -th element, and \vec{g}^e the temperature gradient whose components are given by:

$$g_x^e = \frac{y_j - y_k}{2A_e} T_i + \frac{y_k - y_i}{2A_e} T_j + \frac{y_i - y_j}{2A_e} T_k \quad (4)$$

$$g_y^e = \frac{x_k - x_j}{2A_e} T_i + \frac{x_i - x_k}{2A_e} T_j + \frac{x_j - x_i}{2A_e} T_k \quad (5)$$

in which T_i, T_j, T_k are the node temperatures, $x_i, x_j, x_k, y_i, y_j, y_k$ the node coordinates, and A^e the area of the element. The area vectors have the following components:

$$A_{ik,x}^e = -\frac{y_i + y_j + y_k}{3} + \frac{y_i + y_k}{2} \quad (6)$$

$$A_{ik,y}^e = +\frac{x_i + x_j + x_k}{3} - \frac{x_i + x_k}{2} \quad (7)$$

$$A_{ij,x}^e = -\frac{y_i + y_j + y_k}{3} + \frac{y_i + y_j}{2} \quad (8)$$

$$A_{ij,y}^e = +\frac{x_i + x_j + x_k}{3} - \frac{x_i + x_j}{2} \quad (9)$$

Eq. (3) contains two source terms: ϕ_i^p is the energy production term inside the polygon associated with the i -th node, while ϕ_i^c is the energy flux coming from a boundary polygon.

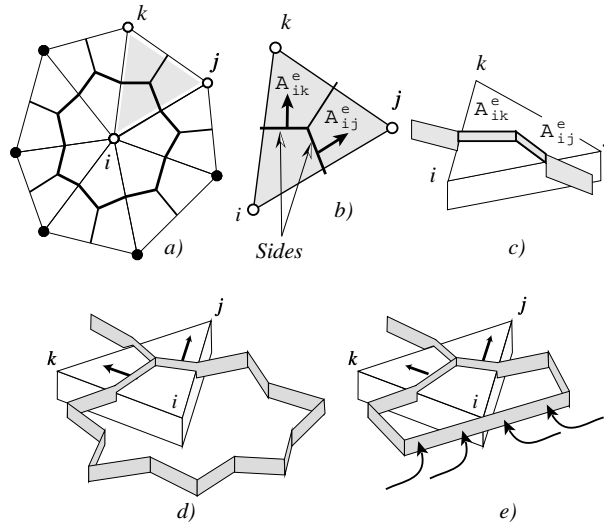


Fig. 2. Tributary areas and related area vectors: a) tributary region obtained with barycenters and midpoints of the sides; b) triangular element containing two sides of the dual mesh; c) area vectors; d) a complete dual polygon; e) an incomplete dual polygon, occurring when the i -th node lays on the boundary.

3. The meshless approach

Considerations done in previous sections show how the key-point in the Cell Method is represented by the determination of the tributary region for each node. Thus, it is evident that the global mesh is redundant since, for each node, only the local primal mesh is of importance, from which the local dual mesh (and hence the tributary

area) can be generated. In this way, it may happen that some local meshes (and tributary regions) overlap, but this is actually of no matter, since we are dealing with conservation equations and, if equilibrium is guaranteed on a domain, it is also satisfied on every subdomain, independently of its shape and/or direction (provided that the union of such tributary areas is equal to or greater than the whole domain). This simple principle is sometimes disregarded, especially due to the fact that Finite Element and Finite Volume Methods rely on cartesian reference systems and on an exact covering of the computational domain with a global mesh.

The meshless approach, on the contrary, is based on the construction of a local mesh and the tributary region of only one node at a time. The implemented algorithm is conceptually very simple, and is made up of three stages, that is:

- (i) for each node i , N border nodes (i.e., its nearest nodes) are selected, with N ranging between four and eight (simulations carried out with higher numbers usually resulted in a deformed local mesh);
- (ii) these N nodes are sorted in an anticlockwise fashion, based on the angle that the segment joining the i -th node and the generic border node makes with a reference direction;
- (iii) the local primal mesh is generated: it is made up of the triangles whose vertices are the i -th node and its border nodes;
- (iv) the polygon of influence of the i -th node is finally constructed: its sides are the segments joining the baricenters of the triangles with the midpoints of their sides.

The fundamental matrix, whose a precise definition can be found in Tonti (2001), is determined by applying such algorithm and Eq. (3) to all nodes.¹ Fig. 3 represents some local meshes generated with a different number of border nodes.

The algorithm described is characterized by ease in implementation and in posing Dirichlet and Neumann boundary conditions. On the other hand, posing boundary conditions with a meshless approach in Finite Element Methods would require the solution of several problems, for which various authors proposed different (more or less elaborated) stratagems. The complexity arises from the fact that, in a meshless approach, the shape function does not exactly fulfils nodal values, but only in an average sense, through a least-squares interpolation. As an example, some researchers have considered a thin domain on the boundary, on which the classical discretization approach is applied, while others have adopted a modified collocation method and a penalty formulation to solve the problem.^{11,13}

The meshless approach with the Cell Method here adopted relies on a linear interpolation on every triangle of the local mesh of the i -th node, thus exactly fulfilling the nodal value. In this way, no restriction arises when imposing Dirichlet boundary conditions. As for natural boundary conditions, there are no problems at all: from Eq. (3), the term ϕ_i^e is the energy flux coming from the boundary of the polygon associated with the i -th node and represents the Neumann boundary condition in global terms.

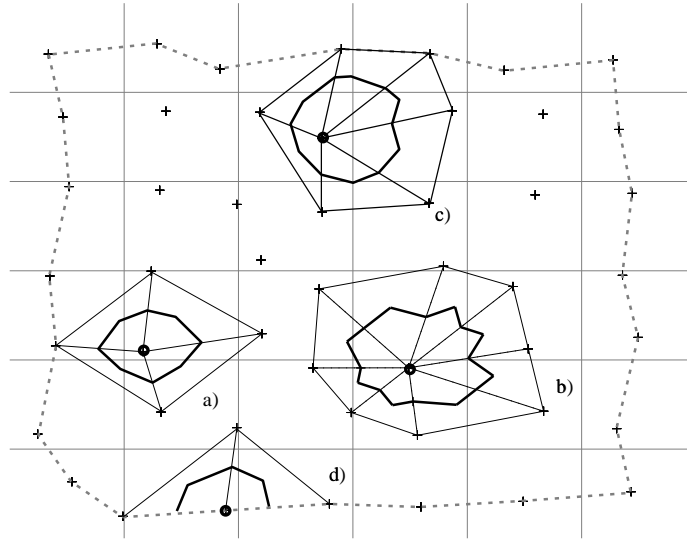


Fig. 3. Generation of local meshes and influence polygons: nodes are represented by a + sign, and the dotted line identifies the boundary. In a), b) and c) the local mesh is generated with four, eight and six border nodes, respectively; d) example of local mesh and tributary polygon for a boundary node: in this case, numerical analyses have shown that three border nodes represent the optimal choice.

4. Some investigations

Numerical analyses have been focused on the Laplace equation, $\Delta^2\phi = 0$, on the domain $\Omega = (0, 5) \times (0, 5)$, and have assumed the harmonic functions reported on Tab. 1 (recall that the real part of any complex variable function is itself a harmonic function). Boundary conditions, both natural and essential, have been derived directly from analytical solution.

Table 1. Harmonic functions adopted in the numerical analyses.

Function name	Analytical expression
F1	$\text{Re } \sin(z)$
F2	$\text{Re } \sqrt{z}$
F3	$\text{Re } \sinh(z)$
F4	$\text{Re } z \sin(z)$
F5	$\text{Re } e^{-z}$
F6	$\text{Re } z e^{-z}$
F7	$\text{Re } z^2 e^{-z}$
F8	$\text{Re } \log(z + 3)$
F9	$\text{Re } e^{-z} \sin(z/10)$
F10	$\text{Re } \cos(z/10) \sin(z/10)$
F11	$\text{Re } \cosh(z)$
F12	$\text{Re } \cos \left[z^3 + \frac{1}{(z+1)^2} + z \right]$

All numerical runs have been carried out with the aim of investigating:

- (i) the convergence order with regular grids and essential boundary conditions;

- (ii) the accuracy obtained when varying the number of border nodes belonging to the local mesh (with regular and irregular grids, and essential boundary conditions);
- (iii) the sensitivity with respect to boundary conditions and grid type (regular or irregular).

In the following paragraphs, results of the analyses are reported.

4.1. Convergence order with regular grids and essential boundary conditions

For regular grids (that is, grids of points equally distributed in space along x and y directions), the numerical scheme has a convergence of second order, and does not depend on the number of border nodes. To prove this, it suffices to consider the i -th row of the fundamental matrix, which is identical to the row one would obtain using the Finite Difference discretization with a five point molecule (see Appendix B). We can then speak of a generalization of Finite Differences, and some authors have proposed to extend the FD method also to unstructured grids, although the starting point is a differential (and not discrete) formulation.¹⁶

Fig. 4 shows the root mean square error, rms , as a function of grid size, Δh , and harmonic function type: note how angular coefficients assume, on average, a value of two (they vary between 1.81 and 2.20). In all the runs, Dirichlet boundary conditions have been adopted.

4.2. Accuracy depending on the number of border nodes

Numerical experiments carried out with Dirichlet boundary conditions and for regular grids have shown that the number of border nodes has no influence on the order and on the accuracy of the scheme. To understand this, consider Fig. 5, in which two adjacent triangles are highlighted: using equations (3)-(9), and after some manipulations, the contribution of the triangle ijk to the flux for the i -th node is given by:

$$\phi = \frac{y_k - y_j}{2} \frac{T_j - T_i}{x_j - x_i} \quad (10)$$

The same can be done for the other triangle, ikm , whose contribution to the flux is:

$$\phi = \frac{x_k - x_m}{2} \frac{T_m - T_i}{y_m - y_i} \quad (11)$$

From the above relations, it is evident that there is no contribution to the conservation equation (and hence to the fundamental matrix) from node k .

On the other hand, the number of border nodes has a strong influence on the results obtained for the case of irregular grids. Fig. 6 shows the root mean square error as a function of mean grid size, $\Delta h_{\text{average}}$, and the number of border nodes for harmonic function F9: from the figure, it is evident the improvement in the solution when increasing the number of border nodes and the number of grid points. In all

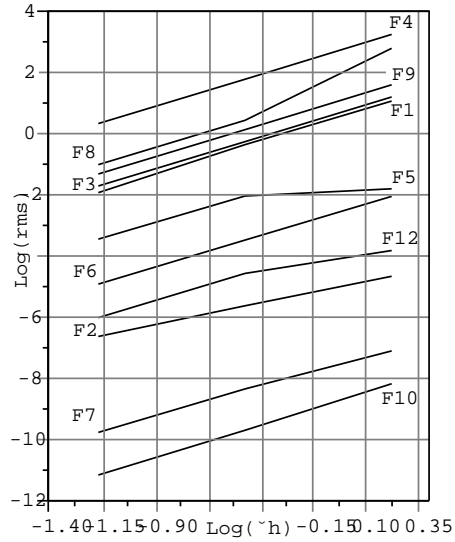


Fig. 4. Root mean square error, rms , as a function of grid size, Δh , and harmonic function type (F1 - F11, see Tab. 1), in presence of Dirichlet boundary conditions and for regular grids. Convergence order of the scheme, represented by the angular coefficient of the lines, varies between 1.81 and 2.20. Line F11 is not reported, being coincident with F3.

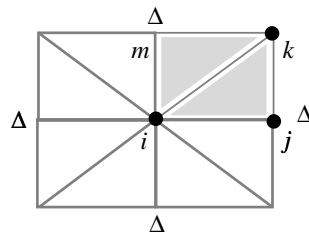


Fig. 5. Regular grid and triangular local mesh: only the nodes identified with Δ give contribution to the conservation equation (and to the fundamental matrix) written for node i .

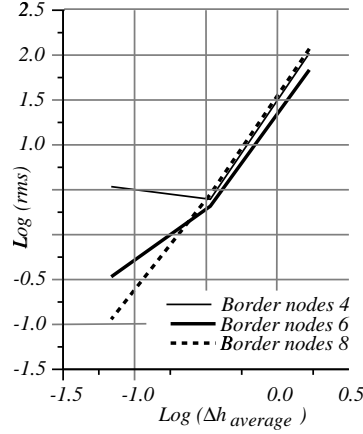


Fig. 6. Root mean square error, rms , as a function of mean grid size, $\Delta h_{average}$, and number of border nodes for harmonic function F9, in presence of Dirichlet boundary conditions and for irregular grids. Convergence order of the scheme, represented by the angular coefficient of the lines, is 2.11 in all cases.

the cases considered (number of border nodes varying from four to eight), the final value of the convergence order was 2.11.

4.3. Sensitivity with respect to boundary conditions and grid type

In this last group of experiments, the objective was to analyze the behaviour of the method with respect to changes in boundary conditions.

The numerical tests have shown that, both for regular and for irregular grids, the presence of essential and natural boundary conditions does not alter the convergence order, as represented in Fig. 7, in which the root mean square error is plotted for regular and irregular grids for harmonic function F9 and for Neumann and Dirichlet boundary conditions. For regular grids, a value of 1.90 has been obtained, while for irregular grids a convergence order of 2.11 has been achieved.

5. A further simplification in the determination of the tributary area

The algorithm described in section 3 can be drastically simplified if we keep in mind the following considerations:

- (i) in the Cell Method, no restriction is imposed on the determination of the tributary area: as already mentioned in section 2, it can be formed using the barycenter, the circumcenter or the incenter, but also any other point inside the triangle may be chosen, even a random one;
- (ii) it can be shown that, whatever the points selected in constructing the tributary region, the fundamental matrix is always the same (see Appendix A);

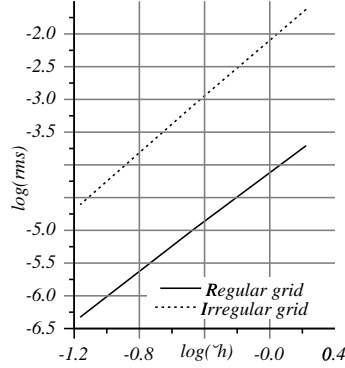


Fig. 7. Root mean square error, rms , as a function of grid size, Δh , and grid type (regular or irregular) for harmonic function F9, in presence of Dirichlet and Neumann boundary conditions. Convergence order of the scheme, represented by the angular coefficient of the lines, is 1.90 for regular grids (solid line) and 2.11 for irregular ones (dotted line).

- (iii) the shape of the tributary area tends to be circular when increasing the number of border nodes; Fig. 8 shows an example, when the circumcenters of the triangles are used, both for regular (Fig. 8a) and for irregular (Fig. 8b) grids.

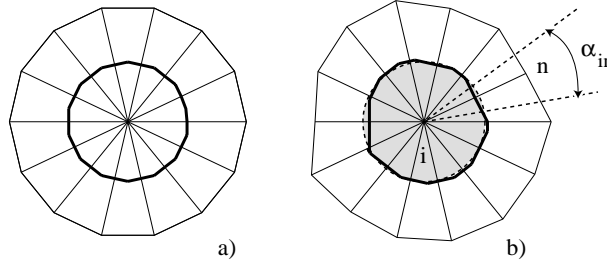


Fig. 8. Tributary regions obtained using the circumcenters of the triangles: it is easily seen that, for an increasing number of border nodes, the shape of the tributary area tends to be circular, both for regular (a) and for irregular (b) grids. In (b), the angle α_{in} used to determine the circular sector belonging to side $i-n$ is represented, calculated using the bisectors with adjacent sides.

To construct the tributary circle for node i , steps (i) and (ii) of the algorithm are first performed (using a higher number of border nodes). Then, for each side connecting node i with a border node n , a tributary sector is chosen, whose amplitude is given by the angle α_{in} between the bisectors with adjacent sides, Fig. 8b. The sum of all such sectors is obviously the tributary area of node i .

This procedure is much easier than that illustrated in section 3, and has the

great advantage of simplifying considerably the Poisson equation, which becomes

$$-\sum_{n \in \mathcal{J}(i)} k \left(R_i \frac{T_n - T_i}{L_{in}} \alpha_{in} \right) = \phi_i^c + \phi_i^p \quad (12)$$

in which L_{in} is the length of side $i-n$, T_i and T_n the temperatures of nodes i and n , and R_i is the radius of the circle, which has been chosen as half of the average of all side lengths:

$$R_i = \frac{1}{2N} \sum_{k \in \mathcal{J}(i)} L_{ik} \quad (13)$$

where, as usual, N is the number of border nodes.

Numerical runs carried out for both regular and irregular grids (using the same harmonic functions listed on Tab. 1) have shown that the methodology has the same accuracy and order of convergence as the previous one, but its efficiency becomes evident when handling situations with very irregular grids. As an example, Fig. 9 represents a grid generated with a random distribution of points.

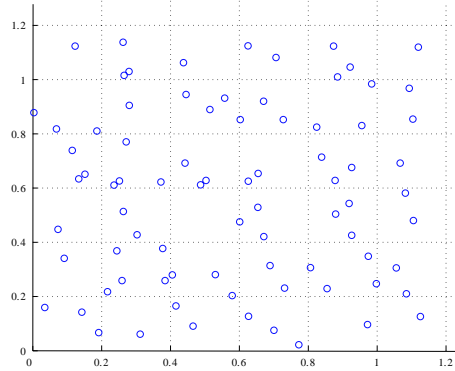


Fig. 9. Irregular grid generated using a random distribution of points.

Eq. (12) has been solved on such grid, using harmonic function F1 for the comparisons. Fig. 10 reports the results obtained, from which it can be seen that numerical solution (represented by cross dots) is very close to the analytical one (small circles).

6. Concluding remarks

The paper has presented a new approach for the numerical integration of partial differential equations representing conservation laws in many engineering and physics fields. The procedure has been described in detail for the Laplace equation, together with the analysis of the convergence order. The main idea on which it is based is the writing of the governing equations directly in a discrete form over

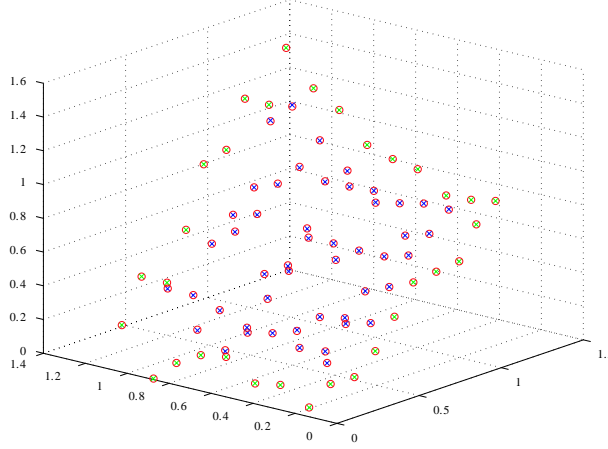


Fig. 10. Comparison between analytical solution (small circles) and numerical results (cross dots) obtained on the irregular grid shown on Fig. 10 using harmonic function F1 reported on Tab. 1.

tributary areas identified, for each node, by a local mesh generated using only a number of neighboring nodes. This way of acting is based on the simple principle according to which if equilibrium is guaranteed on a domain, it is also satisfied on every subdomain, provided that the former is contained in the union of all tributary areas. The proposed approach avoids global mesh generation (which can be a very time-consuming process in problems like fracture propagation) and is characterized by ease in implementation and in posing Dirichlet and Neumann boundary conditions, thus eliminating some problems typically encountered in FEM. Moreover, the choice of circles as tributary regions allows a considerable simplification in writing the discrete form of the governing equations, while maintaining the same accuracy and order of convergence, but also with enhanced performances in the presence of very irregular grids.

Appendix A

Referring to Fig. A.1.a, and considering the triangle formed by the points i, j , and k , the coordinates of its vertices are: node i $(0,0)$; node j $(x_j,0)$; node k (x_k, y_k) . If we consider the temperature T over the nodes (i.e. T_i, T_j, T_k), the linear interpolation $f(x, y)$ over the triangular element is given by

$$f(x, y) = T_i + (T_j - T_i) \frac{x}{x_j} + \left(T_i \frac{x_k - x_j}{x_j} - T_j \frac{x_k}{x_j} + T_k \right) \frac{y}{y_k} \quad (\text{A.1})$$

and the gradient vector is expressed as

$$\nabla f = \left[(T_j - T_i) \frac{1}{x_j}, \left(T_i \frac{x_k - x_j}{x_j} - T_j \frac{x_k}{x_j} + T_k \right) \frac{1}{y_k} \right] \quad (\text{A.2})$$

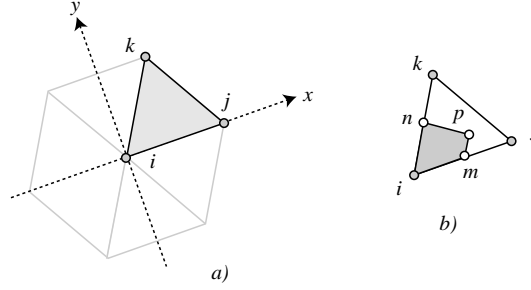


Fig. A.1. Triangular element used for determining the flux: a) coordinate system adopted with x -axis along nodes i and j of the triangular element; b) tributary region of node i belonging to triangle ijk : p is any point inside triangle ijk , while m and n are the midpoints of sides ij and ik , respectively.

If we consider a point p inside triangle ijk (Fig. A.1.b), whose coordinates are

$$x_p = \alpha x_j + \gamma x_k \quad (\text{A.3})$$

$$y_p = \gamma y_k \quad (\text{A.4})$$

where $\alpha \leq 1$, $\gamma \leq 1$, and $\alpha + \gamma = 1$, the flux ϕ through the polygonal joining points m (midpoint of side ij), p , and n (midpoint of side ik) is given by

$$\phi = \vec{v}_{mp} \cdot \nabla f + \vec{v}_{pn} \cdot \nabla f \quad (\text{A.5})$$

in which \vec{v}_{mp} and \vec{v}_{pn} are the area vectors expressed as

$$\vec{v}_{mp} = \left[y_p, -\left(x_p - \frac{x_j}{2}\right) \right] \quad (\text{A.6})$$

$$\vec{v}_{pn} = \left[\left(\frac{y_k}{2} - y_p\right), -\left(\frac{x_k}{2} - x_p\right) \right] \quad (\text{A.7})$$

Substituting these equations in Eq. (A.5), the flux ϕ is obtained as

$$\phi = (T_j - T_i) \frac{y_k}{2x_j} + \left(T_i \frac{x_k - x_j}{x_j} - T_j \frac{x_k}{x_j} + T_k \right) \frac{1}{y_k} \left(\frac{x_j}{2} - \frac{x_k}{2} \right) \quad (\text{A.8})$$

which shows that ϕ is independent from α and γ . It can be concluded that, if linear interpolation is assumed, the flux through a polygonal passing through the midpoint of side ij , an inner point p , and the midpoint of side ik is independent from the inner point p , and thus the choice of p as the barycenter, the circumcenter, or the incenter of the triangle does not affect the final expression of the fundamental matrix.

Appendix B

If we look at Fig. B.1.a, where a regular grid with $dx = dy = 1$ has been assumed, and take into consideration the four triangles formed by the five points $i(0, 0), j(1, 0), k(0, 1), m(-1, 0), n(0, -1)$, applying repeatedly Eq. (A.8), we can determine the flux through the boundary of tributary region of node i . Denoting with ϕ_{ijk} the flux relative to triangle ijk (and similar for other triangles), for every triangle we obtain the following fluxes:

$$\phi_{ijk} = \frac{T_j + T_k}{2} - T_i \quad (\text{B.1})$$

$$\phi_{ikm} = \frac{T_k + T_m}{2} - T_i \quad (\text{B.2})$$

$$\phi_{imn} = \frac{T_m + T_n}{2} - T_i \quad (\text{B.3})$$

$$\phi_{inj} = \frac{T_n + T_j}{2} - T_i \quad (\text{B.4})$$

and the total flux ϕ_T is given by the sum of all the preceding ones, that is:

$$\phi_T = \phi_{ijk} + \phi_{ikm} + \phi_{imn} + \phi_{inj} = T_j + T_k + T_m + T_n - 4T_i \quad (\text{B.5})$$

which represents the classical five-point Finite Difference scheme (under the hypothesis of linear interpolation).

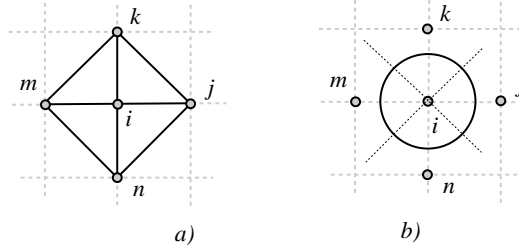


Fig. B.1. Uniform rectangular grid for determining the flux: a) triangular elements related to node i ; b) tributary circle of node i .

The same result can be obtained adopting the simplified approach, in which the tributary circle is considered (Fig. B.1.b): the total flux through the four circular sectors is expressed as:

$$\phi_T = \frac{\pi}{2} R \left(\frac{T_j - T_i}{L_{ij}} + \frac{T_k - T_i}{L_{ik}} + \frac{T_m - T_i}{L_{im}} + \frac{T_n - T_i}{L_{in}} \right) \quad (\text{B.6})$$

in which $L_{ij}, L_{ik}, L_{im}, L_{in}$ are the distances between points, which are all equal to unity due to the choice of the grid. The total flux is then proportional to:

$$\phi_T \propto T_j + T_k + T_m + T_n - 4T_i \quad (\text{B.7})$$

References

1. E. Tonti, *Journal of Computer Modeling in Engineering and Sciences, CMES*, **2** (2), 2001, pp. 237-258.
2. E. Tonti, *Journal of Computational Acoustics*, **9** (4), 2001, pp. 1355-1382.
3. E. Tonti, *IEEE Transactions on Magnetics*, **38** (2), 2002, pp. 333-336.
4. K. M. Liew, Y. Q. Huang and J. N. Reddy, *International Journal of Computational Engineering Science*, **3** (1), 2002, pp. 1-12.
5. J. Ren and K. M. Liew, *International Journal of Computational Engineering Science*, **3** (2), 2002, pp. 219-233.
6. K. M. Liew, H. K. Lim, M. J. Tan and X. Q. He, *Computational Mechanics*, **29** (6), 2002, pp. 486-497.
7. K. M. Liew, T. Y. Ng and Y. C. Wu, *Engineering Structures*, **24** (5), 2002, pp. 543-551.
8. K. M. Liew, T. Y. Ng, X. Zhao and J. N. Reddy, *Computer Methods in Applied Mechanics and Engineering*, **191** (37-38), 2002, pp. 4141-4157.
9. K. M. Liew, H. Y. Wu and T. Y. Ng, *Computational Mechanics*, **28** (5), 2002, pp. 390-400.
10. K. M. Liew, Y. C. Wu, G. P. Zou and T. Y. Ng, *International Journal for Numerical Methods in Engineering*, **55** (6), 2002, pp. 669-683.
11. T. Belytscko et al., *Computer Methods in Applied Mechanics and Engineering*, **139**, 1996, pp. 3-47.
12. S. N. Atluri, H. G. Kim and J. Y. Cho, *Computational mechanics*, **24** (5), 1999, pp. 348-372.
13. T. Zhu and S. N. Atluri, *Computational Mechanics*, **21**, 1998, pp. 211-222.
14. E. Ferretti, E. Viola and A. Di Leo A., "Impiego del metodo delle celle nella stima dei fattori di intensificazione degli sforzi", *Atti XXIX Convegno Nazionale dell'Associazione Italiana per l'Analisi delle Sollecitazioni*, Lucca (Italy), 6-9 settembre 2000, pp. 698-708, in italian.
15. A. Nappi, S. Rajgelj and D. Zaccaria, in *Mesomechanics 2000, Volume I, Proceedings of the Third International Conference for Mesomechanics, Xi'an (China), 13-16 June*, ed. G. C. Sih, pp. 395-406.
16. J. Orkisz, in *Handbook of Computational Solid Mechanics*, ed. M. Kleiber (Springer-Verlag, Berlin, 1998), pp. 336-432.